How can power-to-ammonia be robust? Optimization of an ammonia synthesis plant powered by a wind turbine considering operational uncertainties.

Kevin Verleysen[a,b,*], Diederik Coppitters[a,b,c], Alessandro Parente[b], Ward De Paepe[c], Francesco Contino[a,b],

[a] *Vrije Universiteit Brussel (VUB), Thermo and Fluid dynamics (FLOW), Pleinlaan 2, 1050 Brussels, Belgium*
[b] *Vrije Universiteit Brussel (VUB) and Université Libre de Bruxelles (ULB), Combustion and Robust Optimization Group (BURN), 1050 Brussels, Belgium*
[c] *University of Mons (UMONS), Thermal Engineering and Combustion Unit, Place du parc 20, 7000 Mons, Belgium*

Abstract

The increasing share of wind energy induces a strain on the electricity network. To unburden the transmission system operators from this strain, the dispensable wind energy can locally be stored in an energy carrier, e.g. ammonia (NH_3). Existing work considers fixed operational parameters during design optimization to represent real-life conditions of the Power-to-Ammonia (PtA) system. However, uncertainties significantly affect real-life performances, which can lead to suboptimal plants. To provide a robust design −least sensitive to uncertainties− we considered the main operational uncertainties during design optimization and illustrated the contribution of each uncertainty on the systems NH_3 production. This work presents the optimization under uncertainty of the PtA process and a global sensitivity

*Corresponding author
Email address: kevin.verleysen@vub.ac.be (Kevin Verleysen)

analysis on the optimal designs. The results revealed a design trade-off, where a *productive* design produces 3.2 times more NH_3 on average but is 2.6 times less robust (higher standard deviation) than the *robust* design. A global sensitivity analysis on the most robust design showed that the temperature fluctuation of the NH_3 reactor dominates the average ammonia production by 99.7%, while the wind speed measurement error and the temperature variation both influence the ammonia production of the most productive design by 75.4% and 22.5%. Accordingly, an accurate anemometer and improving the temperature control over the NH_3 reactor are the most effective actions to make the most productive design more robust. However a robust plant can be obtained by decreasing the load size of the plant, it suffices improving the temperature control over the NH_3 reactor to make this design (adopted from the trade-off) less sensitive to the noise. Future investigations involve analyzing the dynamical operations of the robust PtA pathway and analyze the impact of uncertainties on its levelized cost.

Keywords: Power-to-ammonia, Robust design optimization, Haber-Bosch synthesis, Seasonal hydrogen storage, Energy storage system

1. Introduction

The erratic nature of renewable sources requires a higher degree of flexibility of the electricity grid [1]. To avoid this requirement, an energy storage system is necessary to regulate the supply of this non-dispatchable energy, removing its intermittent effect on the grid. The primary purpose of the storage system is to capture the excess energy at any time and inject it back into the grid to compensate for variability between supply and demand without

relying on fossil fuels, improving the security of electricity supply in a sustainable way [2, 3]. For significant power levels, the production of chemicals can be employed to store the energy in a electrochemical energy carrier. This energy carrier could subsequently fuel a power production system for power generation; balancing the electricity network for prolonged power disruptions and reduce the need for a flexible grid [4].

The hydrogen-based Power-to-Power (PtP) concept enables the storage of large-scale (∼MW) power via water electrolysis, but realizing it in practice is proven difficult. The interest in environmental concerns increased in recent years, which helped to lower the cost of renewable energy technologies. This economic trend promoted the creation of numerous research and demonstration projects across Europe [5, 6, 7, 8]. However, storing pure H_2 in a compressed or cryogenic (below -253°C) container for several months provides low PtP efficiencies (between 34% and 38%) [9]. Besides, the storage of this substance initiates safety issues [10, 11]. A more viable and safer way for the implementation of this hydrogen-based energy storage system is by converting the electrolytic H_2 to ammonia (NH_3), using the industrially mature Haber-Bosch Synthesis (HBS) process [12]. The HBS process consists of synthesizing a mixture of H_2 and nitrogen gas (N_2) to form NH_3 in the presence of a catalyst at an operational temperature between 350°C and 550°C and a pressure ranging from 150 bar to 250 bar [13, 14, 15].

NH_3 gained a significant role during recent years in the application of large-scale H_2 storage, but also for its potential utilization as a maritime fuel and sustainable nitrogen-based fertilizer [16, 17, 18, 19, 20]. Morgan et al. [13] developed an analytic model to determine in which circumstances this

concept of Power-to-Ammonia (PtA) can be economically viable in addition to a diesel-fueled generator for a geographic islanded case. A more extensive analysis by Bañares-Alcántara et al. investigated the potential use of the NH_3-based energy storage in electric islanded cases [14]. Later on, the Institute for Sustainable Process Technology (ISPT) presented a feasibility study for implementing this renewable NH_3 concept of storing the abundance of wind energy for local farming and power generation in the Netherlands by considering economic and industrial competitive scenarios [9]. The presence of uncertainties are however observed by Reese et al. on the operations of a small-scale ammonia synthesis pilot plant located in Minnesota, in the form of temperature and pressure fluctuations in the reactor [17]. Although these studies each included a sensitivity analysis of the operations of the electrolyzers and the HBS process, no investigation has been done on the identification and quantification of operational uncertainties influencing the performance of the entire storage system design.

This paper provides the modeling of the NH_3-based energy storage together with the identification of reported operational uncertainties from literature, which was combined to ultimately preform a design optimization under uncertainties. We performed consecutively the modeling in Aspen Plus of an electrolyzer operating with an alkaline electrolyte, a Pressure Swing Adsorption (PSA) to obtain nitrogen from air, and a Haber-Bosch Synthesis (HBS) plant to synthesize NH_3. In addition to the chemical modeling in Aspen Plus, a Wind Turbine Generator (WTG) is created in Python to convert wind speed into electric power. These models were assembled and optimized with a Multi-Objective Genetic Algorithm (MOGA) to establish

a set of optimal designs. This energy model was then combined with the identified operational uncertainties of each subsystem to establish an optimization under uncertainty by the use of an Uncertainty Quantification (UQ) algorithm. With the MOGA and UQ approaches, a set of designs was determined which were least sensitive to the effect of these uncertainties while maximizing the NH_3 production. This so-called Robust Design Optimization (RDO) approach robustified the performance of the plant. The RDO process consisted of combining the Nondominated Sorting Genetic Algorithm (NSGA-II) [21] and the Polynomial Chaos Expansion (PCE) technique [22], which ultimately evolved the defined design parameters towards a better performance while taking into account the implemented uncertainties.

2. Modeling the storage of wind energy through ammonia synthesis

This section presents the design of each process necessary to store wind energy in the energy carrier NH_3. The first subsection provides the wind speed data used to power the storage system. This power is determined by the model of a wind turbine in Python. Each following subsection presents the modeling of an Alkaline Water Electrolyzer (AWE), a PSA and the HBS in Aspen Plus. The description and integration of the operational uncertainties are included for the wind turbine model, the AWE and the HBS at each corresponding subsection.

2.1. Wind power generation

We incorporated the hourly wind speed measurement data of a wind turbine park located in Galicia (Spain) and sequentially sorted the data in a wind speed frequency distribution with a step size of 1 m/s [23]. Through

the integration of a power curve of a typical wind turbine model, this wind speed data is converted into electric power. We based this power curve on the design of the Vestas V112 onshore wind turbine and integrated this curve in Python through Equation 1 to calculate the generated wind power (P_{WTG}):

$$P_{\mathrm{WTG}} = \frac{1}{2}\rho A C_P v^3 \qquad [\mathrm{W}], \tag{1}$$

where ρ is the density of air in kg/m^3 (at sea level and at 15$^{\mathrm{o}}$C, $\rho = 1.22$ kg/m^3), A is the area of the rotating blades in m^2, C_P is the power coefficient and v is the wind speed in m/s.

In the adopted model, the maximum power output was adjusted to 3 MW at a rated wind speed of 11 m/s while assuming a constant power coefficient of 37%. We performed this adaptation to correlate the wind speed and electric power between the cut-in and rated wind speed with the cubic relationship (Equation 1) without taking into account the dependency of C_p on the wind speed. The original and adopted design specification are provided in Table 1.

Wind turbines are inherently influenced by a variety of uncertainties, providing ambiguous prospects for start-up wind turbine parks. These uncertainties have a direct effect on the profitability of these projects, which are mainly based on wind speed measurements or estimations to forecast the capacity factor [26] or the Annual Energy Production (AEP) of a location [27]. Lackner et al. categorized a variety of uncertainties influencing this AEP in four categories, which consists of: wind speed measurement uncertainty, historical wind speed data, wind resource modeling variability, and lastly, the site assessment uncertainty [27]. Because the wind speed measurements for

Table 1: Wind turbine generator design specifications, constraints and wind speed measurement uncertainty.

Design specification		Reported value [24]	Adopted value
C_P	[W/W]	$C_P(v)$	37.0
A	[m^2]	9852.0	9852.0
Constraints			
$v_{\text{cut-in}}$	[m/s]	3	3
v_{rated}	[m/s]	12	11
$v_{\text{cut-out}}$	[m/s]	25	25
Uncertainty		Integrated value [25]	
$e_{\text{measurement}}$	[-]	$\pm 1\%$	

one year are used in this design optimization study (not the power production of an actual wind turbine) only the first category of Lackner et al. (the wind speed measurement error) is applied to the design of the WTG and furthermore considered in the UQ analysis. Kaganov et al. designated the wind speed measurement error of rotational measurement devices between 1% and 6% [25]. We choose to integrate a wind speed uncertainty of 1% to consider the most accurate wind speed measurement in the wind turbine design. This uncertainty is characterized by a Gaussian distribution in the UQ analysis which assess for each design the uncertainty propagation on the considered objective. The following expression enables the implementation of this uncertainty (Equation 2):

$$v_{\text{measurement}} = v_{\text{data}}(1 - e_{\text{measurement}}) \qquad [\text{m/s}], \tag{2}$$

where $v_{\text{measurement}}$ is the measured wind speed in m/s resulted from the input wind data (v_{data}) and the error of the device ($e_{\text{measurement}}$) in %. During the robust design process, the measured wind speed ($v_{\text{measurement}}$) replaces the wind speed (v) in Equation 1.

2.2. Alkaline water electrolyzer

An Alkaline Water Electrolyzer (AWE) was selected because of its proven reliability in industrial applications and a multitude of commercially available technologies on the market, allowing the AWE to operate commercially at MW scale [15, 28, 29]. The AWE process was modeled in Aspen Plus for one electrolytic cell (Figure 1). To resemble the real operation of an AWE and determine the hydrogen production when applying electric power to the electrolyzer stack, the electrolyzer model of Ulleberg [30] is integrated with a FORTRAN calculator in the 'Electrolytic cell' block (Figure 1). Ullebergs electrolyzer model consists of two empirical equations: a voltage-current (U-I) relationship and the characterization of the Faraday efficiency (η_{F}).

The applied voltage U on the electrolytic cell is determined by the reversible voltage U_{rev} of the electrolytic reaction, the current I flowing through the electrolytic cell and T the operational temperature of the electrolytic cell. This relationship is defined with the following expression [30]:

$$\begin{aligned} U_{\text{real}} = & U_{\text{rev}} + (r_1 + r_2 T)\frac{I}{A} \\ & + (s_1 + s_2 T + s_3 T^2) \log\left((t_1 + t_2/T + t_3/T^2)\frac{I}{A} + 1\right) \ \text{[V]}, \end{aligned} \tag{3}$$

where r_i are the parameters related to the ohmic resistance of the electrolyte (for i = 1,2), s_i and t_i are the coefficients for overvoltage on the electrodes

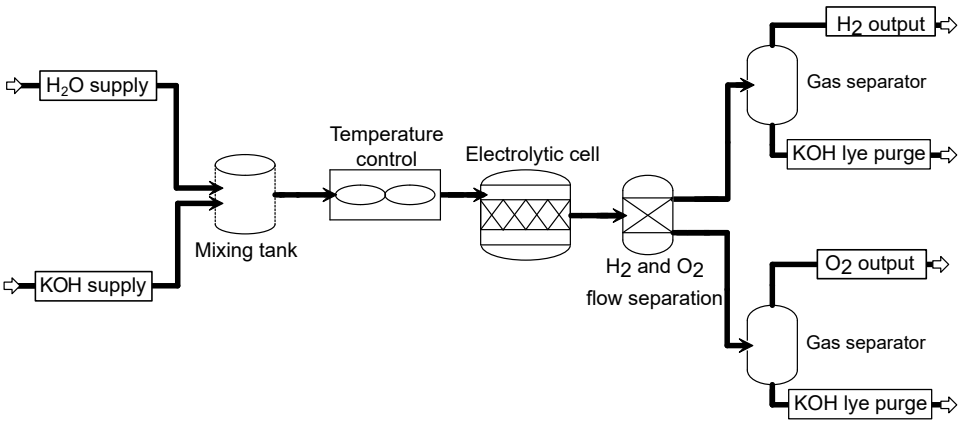

Figure 1: In the Aspen Plus model of the alkaline electrolyzer, KOH lye is dissolved in a tank with water (H_2O), where its exothermic reaction increases the temperature of the mixture. A heat exchanger controls the temperature of the alkaline solution flowing to the electrolytic cell. The block components of one electrolytic cell and the product separation creates the H_2 and O_2 flows. The gas separation blocks separate the H_2 gas and KOH mixture, where the same process occurs on the O_2 production side.

(for i = 1,2,3) and A the surface area of the electrodes in m^2. Ulleberg determined the value of these parameters (r_i, s_i and t_i) by a non-linear regression deterministic process (see Table A.4) [30].

The amount of hydrogen produced by the electrolyzer is determined with Faraday's law. This law states that the molar flow rate of the produced hydrogen ($\dot{n}_{H_2}$) depends on the total number of electrolytic cells N and the transfer rate of electrons (Equation 4) [30]:

$$\dot{n}_{H_2} = \eta_F \frac{NI}{zF} \qquad [\text{mol/s}], \tag{4}$$

where η_F is the Faraday efficiency of the electrolytic reaction. This Faraday efficiency expresses the ratio of the flow rate of hydrogen that is produced

by the alkaline electrolyzer, over the theoretical production rate. This ratio is expressed by the second empirical formula with Equation 5 [30]:

$$\eta_{\mathrm{F}} = f_1 \exp\Big(\frac{f_2 + f_3 T}{I/A} + \frac{f_4 + f_5 T}{(I/A)^2}\Big) \qquad [-], \tag{5}$$

where f_i (for i = 1,...,5) are the parameters defining the evolution of the Faraday efficiency, determined by the same non-linear regression process used in Equation 3 at an operational pressure of 7 bar (Table A.4) [30].

Mori et al. studied the steady-state operations of an alkaline electrolyzer, where a sinusoidal behavior of the cell temperature is observed. This temperature varied with a range of $\pm 3^o$C from the desired temperature [31]. The study acknowledged that the heat exchanger controlling the temperature causes this variation in temperature. When implementing this variation in the temperature control block of the AWE Aspen Plus model, the Faraday efficiency (Equation 5) and cell current (through the U-I relationship defined with Equation 3) are affected by this uncertainty, resulting in a variance of hydrogen production (Equation 4). This operational uncertainty is therefore included during the global sensitivity analysis and the robust optimization within this study. The UQ analysis assesses the effect of the variation of the cell temperature for each GA-generated design on the investigated output.

2.3. Pressure swing adsorption

The Pressure Swing Adsorption (PSA) process is selected to obtain nitrogen from the air. Frattini et al. proposed a simplified model of the PSA process in Aspen Plus®, where the design incorporates a single stage compressor, to pressurize the air flow (consisting of 75.5 wt% N_2), and a separation block, to obtain nitrogen [15]. The same philosophy has been used in

Morgan et al. for a mathematical model of a wind-powered ammonia plant in steady-state operations [13]. The nitrogen production depended in both cases on the delivered power to the PSA compressor, which can be expressed with the following relationship between the power P_{PSA} and the air mass flow rate $\dot{m}_{\mathrm{air}}$ [13]:

$$P_{\mathrm{PSA}} = \frac{\dot{m}_{\mathrm{air}}}{\eta_{is}\eta_{\mathrm{mech}}}\Big(\frac{k}{k-1}\Big)T_{\mathrm{in}}R\left[\left[\frac{p_{\mathrm{out}}}{p_{\mathrm{in}}}\right]^{\frac{(k-1)}{k}} - 1\right] \qquad [\mathrm{W}], \tag{6}$$

where η_{is} is the isentropic efficiency ($\eta_{is} = 0.75$ [13]), η_{mech} the mechanical efficiency ($\eta_{\mathrm{mech}} = 0.95$ [13]), T_{in} the inlet temperature in K, R the gas constant of air in J/kgK, k the heat capacity ratio ($k = 1.4$), p_{out} the outlet pressure in bar ($p_{\mathrm{out}} = 7$ bar), and p_{in} the inlet pressure in bar ($p_{\mathrm{in}} = 1$ bar). The mass flow of air ($\dot{m}_{\mathrm{air}}$) is split into a pure mass flow nitrogen and a residual flow of O_2 and Ar by a separation block in Aspen Plus®. The compressor and separator block in Aspen Plus® uses the PENG-ROB property method, which is based on the Peng-Robinson cubic equation of state [15].

2.4. Haber-Bosch synthesis process

An ammonia synthesis design is adopted from the paper of Frattini et al. to replicate the Haber-Bosch Synthesis (HBS) process performance [15]. In the first stage of modeling the ammonia process, the block specifications provided by the paper are implemented in Aspen Plus® (Figure 2) [15]. In the subsequent step, we simplified the Haber-Bosch synthesis loop to reduce the computational cost while creating a single link between the generated wind power and the performance of the HBS process. This model reduc-

tion enabled us to govern the process by a single control parameter. To reach this necessary simplification, several adaptations were applied to the HBS loop of Frattini et al. [15]. Frattini et al. originally integrated pressure losses through the use of the tube-and-shell designs in the integrated heat exchangers (Preheater and Heater in Figure 2) [15]. These pressure losses were discarded from the model, so the reactor compressor which compensated for these pressure losses could therefore be excluded from the model. This model reduction results in the exclusion of the energy consumption of the ammonia synthesis loop. A second modification on the adopted model is the removal of the conditioning block, where water particles from the air or the electrolyzer are cleansed from the flow entering the synthesis loop (Figure 2). Because of the absence of water in both flows, we excluded this condition block from the model. We considered as well pure hydrogen and nitrogen flow rates from the AWE and PSA processes to avoid dealing with the catalyst poisoning caused by the presence of oxygen in both streams, which is a well-reported problem for iron-based catalysts [32]. In industrial processes, a purity of 99.9999% is required with the help of additional purification system to overcome the deactivation of the ammonia synthesis catalyst [32].

These modifications resulted in the use of a single control parameter, namely the direct control over the operational pressure within the synthesis loop through the loop compressor. This loop compressor is sequentially governed by the power supply to this component, as is expressed with Equation 7 for a three stage compressor.

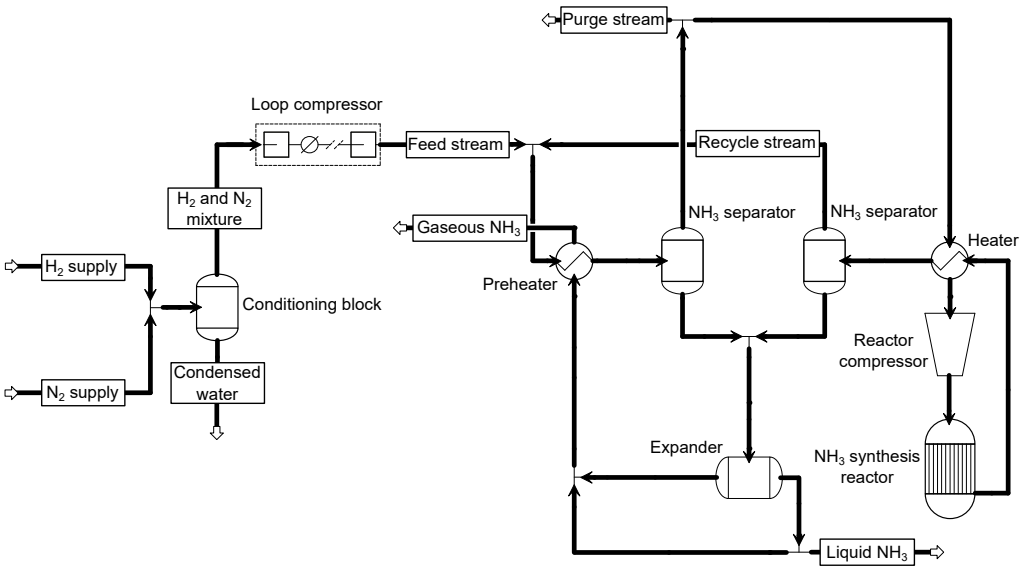

Figure 2: Frattini et al. modeled the Haber-Bosch Synthesis (HBS) loop in Aspen Plus® [15]. In this HBS, the loop compressor pressurizes a mixture of H_2 and N_2 to a certain pressure, where the NH_3 synthesis reactor converts this mixture to NH_3. The ammonia is extracted from the loop through condensation (NH_3 separators).

$$P_{\text{HBS}} = \frac{\dot{m}_{\text{mix}}}{\eta_{is}\eta_{\text{mech}}} \sum_{i=0}^{2} \left(\left(\frac{k}{k-1} \right) T_i R \left[\left[\frac{p_{i+1}}{p_i} \right]^{\frac{(k-1)}{k}} - 1 \right] \right) \qquad [\text{W}] \qquad (7)$$

In this expression, P_{HBS} presents the delivered power to Haber-Bosch compressor in W, $\dot{m}_{\text{mix}}$ the mass flow of gas mixture in kg/s, η_{is} isentropic efficiency, η_{mech} the mechanical efficiency, $T_{\text{in},i}$ inlet temperature of stage i in K (for $i = 0$ to 2), R the gas constant of mixture in J/kgK, k the heat capacity ratio, $p_{\text{in},i}$ the inlet pressure in kPa at stage i in kPa (for $i = 0$ to 2) and $p_{\text{out},i+1}$ the outlet pressure in kPa at stage i in kPa (for $i = 0$ to 2). Frattini et al. provided the design variables of the loop compressor, which is modeled with a MCompr block in Aspen Plus based on the isentropic

compressor model [15]. We compared the HBS power consumption of this simplified process to the reported ammonia synthesis loop in the study of Morgan [33]. This comparison revealed that we obtained very similar results when comparing the relative power consumption in regards to the total power consumption (5.49% with Morgan and 4.44% for our HBS loop). This similar result proves that the applied simplifications is in agreement with another reported PtA energy model.

Operational uncertainties and instability phenomenon in the ammonia synthesis process are described in the literature [17, 34], therefore, disturbances are inherently present in this part of the energy storage model. The paper of Reese et al. acknowledged the presence of uncertainties in practice for a wind-powered ammonia synthesis plant [17]. Although the plant integrated a control system to govern the operations, the measurements of a three-day operation of this plant showed temperature and pressure fluctuations during the steady-state process. The paper interpreted this variability due to the undamped nitrogen supply of the PSA system and the occasional absence of hydrogen coming from the electrolysis process. However, these reported temperature fluctuations are essentially present during the operations and reach up to 50°C [17] without a proper identification or analysis of disturbance. The mathematical model of an ammonia synthesis reactor and a heat exchanger of Jinasena et al. showed also temperature oscillations of this process where a temperature fluctuation of 10°C is present [34]. We included the same reactor temperature fluctuation of ±10°C with a Gaussian distribution within this proposed energy storage model. This uncertainty is set into the operational temperature of the REACTOR block of the Aspen

Plus model. Although pressure fluctuations were also reported in [17], these variations manifested due to erratic flow supply of hydrogen and nitrogen towards the synthesis process, where the origins of the temperature variations were unsubstantiated.

3. Optimization methodology

In this section, the optimization objectives are defined and discussed. The following two subsections designates the design search space and constraints to locate the global optimum within the model constraints. The final part of this section describes the applied MOGA to find these global optimum and the chosen UQ analysis which collectively create the RDO approach. This approach is deemed necessary to maximize the performance of the plant while minimizing the sensitivity of the noise factors on this performance, i.e., robustifying the wind powered ammonia synthesis process.

3.1. Optimization objective

The optimization objectives of this paper were chosen in function of the considered approach (deterministic or robust design optimization). In the Deterministic Design Optimization (DDO) process, the search algorithm maximizes the storage of wind energy in ammonia while conceiving a design able to continuously operate, i.e. maximizing the plants load factor, which provides a higher energy efficiency and ultimately achieve a better economical return on investment [35]. This load factor (L_F), chosen as the second objective, is expressed by the ratio of average consumed power over time (P_{average}) and the plants maximum consumed power ($P_{\text{plant,max}}$) and expressed with Equation 8:

$$L_F = \frac{\sum_{i=1}^{t} P_{\text{plant}}(i)}{P_{\text{plant,max}} t} = \frac{P_{\text{average}}}{P_{\text{plant,max}}} \qquad [-], \tag{8}$$

where P_{plant} is the power consumed by the total plant at a certain time in W and t the time in hours.

In the robust design optimization, the robustification of the ammonia production is opted as the final objective to make it less sensitive to the noise propagation incorporated in the subsystems. We focused on this objective to provide a design which is able to capture the highest amount of wind energy and store it through the production of the studied energy vector while being less influenced by operational uncertainties. This objective is split in two parts, where the average ammonia production needs to be maximized and, secondly, the sensitivity on the ammonia production is minimized. The ratio of the standards deviation (σ) over its average value (μ) of the concerned output characterizes this sensitivity, which is defined in literature as the Coefficient of Variance (CoV). This CoV is expressed in Equation 9 when applied on the ammonia production:

$$\text{CoV} = \frac{\sigma_{\text{NH}_3}}{\mu_{\text{NH}_3}} \qquad [-]. \tag{9}$$

3.2. Design search space

The optimization method enhances the energy storage model according to a wind speed data set while finding the best performing plant design corresponding to the chosen objectives. This best performing design can be reached by searching the best set of design parameters within the defined search space. For attaining this best set, specific design parameters were

selected to optimize the flow of power to each subsystem (AWE, PSA and HBS).

To control the amount of energy captured and converted by the ammonia plant, the simulation disposes of a part of the generated wind power by means of peak shaving; taking the total plant power size as the first design parameter. This captured power is then subdivided into three fractions, where a proportion of power is supplied to the AWE, another part to the PSA and the residual power to the Haber-Bosch compressor to pressurize the ammonia synthesis process. To define the necessary design parameters and attain an optimal configuration among these powers, each of these corresponding subsystems generates hydrogen, nitrogen, and ammonia each at a certain rate. The power sizing of the AWE and PSA are therefore considered as the two successive design parameters, while the power supplied to the HBS compressor is employed as a control parameter (Figure 3). However, a single electrolytic cell can consume a maximum power of 2.1 kW [30], so the stack sizing of the electrolyzer has to be taken into account as well. The number of electrolyzers (N) is therefore selected as the fourth and final design parameter. The candidates generated by the optimization algorithm for this design parameter are rounded up to the nearest integer.

The design search space bounds each design parameter by a minimum and maximum value, so an optimal set of design parameters can be located. For the plant sizing ($\%_{\text{plantsize}}$), the proportion of power flowing to the total ammonia plant can range between 0.001% and 100% according to the 3 MW power capacity of the WTG. This range allows the algorithm to decide which quantity of wind power can be captured by the ammonia plant. The bound-

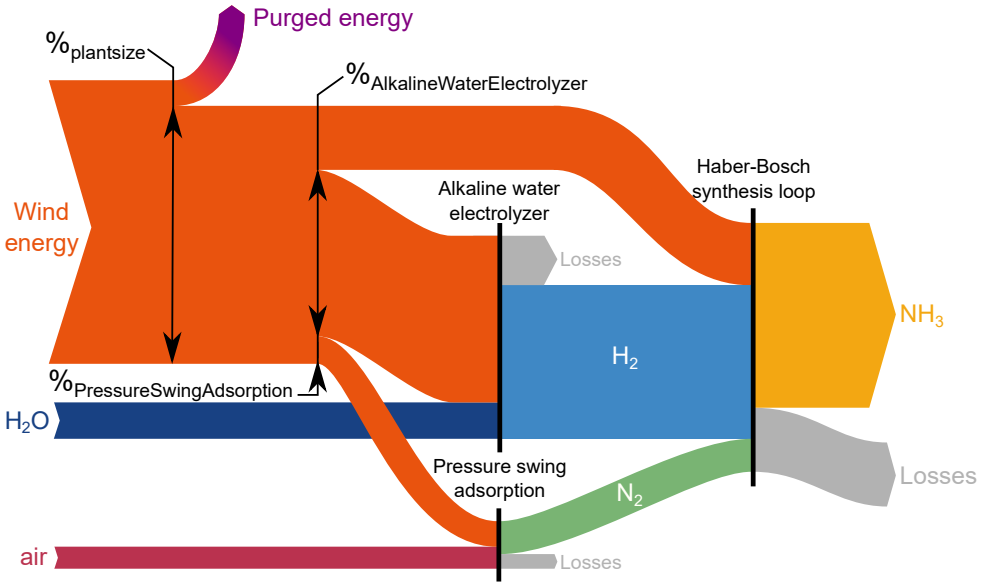

Figure 3: The wind turbine transforms the wind speed into electric power which is then supplied according to a certain ratio to the Alkaline Water Electrolyzer, the Pressure Swing Adsorption and the Haber-Bosch synthesis loop. These processes produces respectively hydrogen, nitrogen and, finally, ammonia through the modeled systems in Aspen Plus. The power ratio towards the individual processes, the plant load size and the numbers of electrolyzers are design parameters defined by the optimization algorithm.

aries of the power proportion of the AWE and PSA ($\%_{\mathrm{AWE}}$ and $\%_{\mathrm{PSA}}$) are selected based on a sensitivity analysis of the Aspen Plus model. The analysis shows that the proportion of power to the AWE varies between 91% and 95% at optimal/stoichiometric conditions (HBS loop pressure of 250 bar and a H_2/N_2 ratio of 3 mol/mol). For the PSA, this parameter varies between 0.9% and 1.6%. We chose a range of 1 and 2600 electrolytic cells to assure the ability of the AWE to perform at an operational power of 3 MW.

3.3. Constraints

Based on the declared restraints by the manufacturer of the alkaline electrolyzer and safety regulations of the ammonia synthesis loop, we constrained three output parameters of the total energy storage model. These three parameters are the current density of the electrolytic cell, the H_2/N_2 ratio entering the HBS compressor and its outlet pressure.

Each electrolytic cell is bounded by a maximum current density of 300 mA/cm^2 [30]. The minimum current density depends on the thermal efficiency (η_{thermal}) which is expressed by Equation 10:

$$\eta_{\text{thermal}} = \frac{U_{\text{tn}}}{U_{\text{real}}} \qquad [-] \tag{10}$$

where U_{tn} is the thermoneutral voltage in V [30].

When the thermal efficiency of the electrolytic cell is higher than 100%, the system requires heat to operate. Because the AWE is a low-temperature electrolyzer, the cell is unable to operate at this point; leading to the elimination of these design parameters from the set of solutions (Figure 4).

The flow towards the Haber-Bosch compressor should consist of a H_2/N_2 ratio between 2 and 3 [33, 36] while the operating pressure lies between 100 and 250 bar [37] (Figure 5). When either of the three output parameters of the model exceeds a limit, the to-be maximized objectives are penalized with a numerical value of 10^{-9} and the minimized outputs (the CoV in the RDO phase) with 10^9. Assigning these numerical values drives the genetic algorithm away from the generated design points and uses the more potent sets of design parameters to evolve towards the best results.

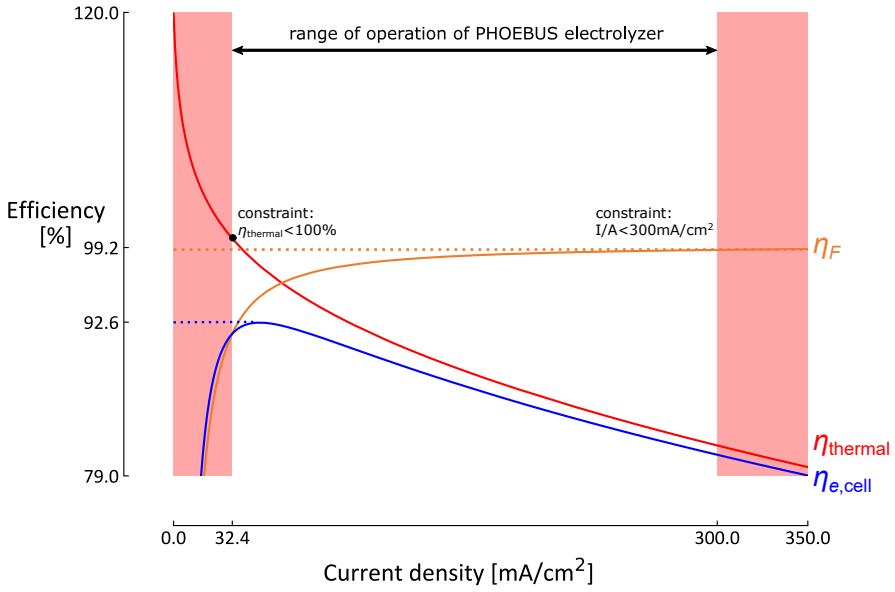

Figure 4: Thermal (η_{thermal}), Faraday (η_{F}) and energy ($\eta_{e,\text{cell}} = \eta_{\text{thermal}}\eta_{\text{F}}$) efficiency of the alkaline electrolyzer in function of the current density at a temperature of 80°C. A peak in the energy efficiency indicates the most optimal point of operation for the electrolyzer to produce H_2 (related to the Faraday efficiency) while a small amount of losses occur (related to the thermal efficiency). The operational range of the electrolyzer is bounded by a minimum and maximum current density.

3.4. Optimization algorithm

To determine the optimal set of design samples for the system model, we implemented the multi-objective Nondominated Sorting Genetic Algorithm (NSGA-II) [21]. First, the algorithm produces an initial set of design samples (n samples) through Latin Hypercube Sampling [38]. Out of this initial design sample set, the algorithm creates a second sample set based on crossover and mutation, with an equal number of samples n. After characterizing both sets of design samples, each design sample is implemented in the system model and evaluated, leading to $2n$ values for each objective. Thereafter,

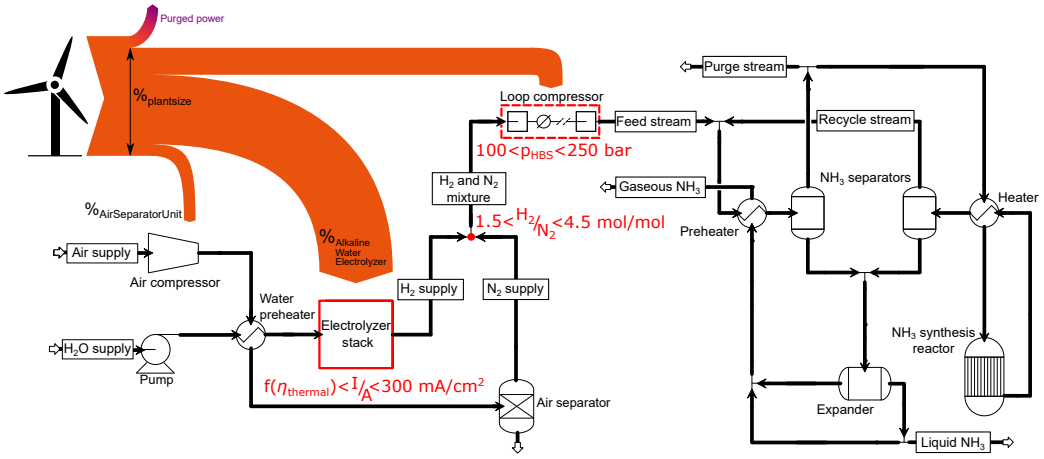

Figure 5: After the optimization algorithm defines the design parameters, a model simulation is executed. A constraint check is then preformed to determine if the suggested design is possible without exceeding the minimum and maximum current density of the individual alkaline electrolytic cell, the H_2/N_2 ratio and the output pressure of the Haber-Bosch loop compressor.

the samples are sorted based on their dominance on the objectives and the n samples with the highest dominance define the second generation of design samples. This iterative process is repeated until a predetermined number of generations is achieved or the simulation converged towards a solution. Depending on the relation between the multiple objectives, the optimal set of design samples can converge to a single optimal design sample (i.e. non-conflicting objectives) or a set of design samples (i.e. conflicting objectives). In such a set of optimal design samples, each sample dominates every other sample in at least one objective (i.e. Pareto frontier).

3.5. Uncertainty quantification method

To propagate the uncertainties of the input parameters through the system model, we implemented the Polynomial Chaos Expansion (PCE) algorithm [39, 40]. This technique provides a computationally efficient alternative for the robust Monte Carlo Simulation technique for a small stochastic dimension (< 10). To quantify the mean and standard deviation of the objective efficiently, the PCE algorithm creates a surrogate model $\hat{M}(\boldsymbol{\xi})$ of the physical model $M(\boldsymbol{\xi})$ based on multivariate orthogonal polynomials Ψ_i and corresponding coefficients u_i:

$$\hat{M}(\boldsymbol{\xi}) = \sum_{i=0}^{P} u_i \Psi_i(\boldsymbol{\xi}) \approx M(\boldsymbol{\xi}). \tag{11}$$

When P in Equation 11 is infinite, the surrogate model is an exact representation of the physical model. In practice, the series is truncated up to a value depending on the complexity of the input-output relation (related to the polynomial order p) and the stochastic dimension d [22]:

$$P + 1 = \frac{(p+d)!}{p!d!}. \tag{12}$$

When the PCE surrogate model is constructed, the mean μ and standard deviation σ follow analytically out of the coefficients:

$$\mu = u_0, \tag{13}$$

$$\sigma = \sum_{i=1}^{P} u_i. \tag{14}$$

Next to the statistical moments of the objective, the contribution of each input parameter to the objective variation can be quantified through Sobol' indices. The first-order Sobol' indices (i.e. no input parameter interaction considered) are defined as:

$$S_i = \frac{D_i}{D} = \frac{\mathrm{Var}[M(\xi_i)]}{\mathrm{Var}[M(\boldsymbol{\xi})]}. \tag{15}$$

Similar to the mean and standard deviation, these first-order Sobol' indices can be quantified analytically via the PCE coefficients:

$$S_i^{PC} = \sum_{\alpha \in A_i} u_\alpha / D \qquad A_i = \alpha \in A : \alpha_i = 0, \alpha_{j \neq i} = 0. \tag{16}$$

4. Results and discussion

This section presents the results and discussion of the DDO and RDO approaches, applied to the power-to-ammonia energy storage system. A global sensitivity analysis applied on the DDO results shows the effect of the uncertainties on the performance of two deterministic optimums. To minimize the effect of the uncertainties on the performance, the RDO approach takes them into account and find a design that can minimize their effects on these results. Again, a global sensitivity analysis is performed on the most relevant designs to show which uncertainties have the most impact on the robustified designs. Finally, we proposed different measures to further reduce the effect of these uncertainties on the RDO results.

4.1. Deterministic design optimization

The deterministic design optimization resulted in a collection of optimal solutions when maximizing the annual NH_3 production and the plants load factor. The NSGA-II algorithm obtained this set of solutions −or Pareto points− due to the conflicting objectives: maximizing $m_{\mathrm{NH_3,total}}$ and L_F. This Pareto front consists of two designs, each configured with two unique design parameters, which enables the optimal performance for a particular objective (Table 2). These two extreme cases are named 'Most NH_3' and 'Best L_F'. Each intermediate set of design parameters between those extremities provides a combination of maximizing both output objectives with a certain weight. The results of the UQ analysis on the two cases show the dominance of the wind speed measurement and the ammonia reactor temperature (Figure 6).

The 'Most NH_3' design enables the highest storage of available wind energy to the energy carrier, ammonia. To obtain this most productive plant, a plant with a load of 2.77 MW (92.4% of the 3 MW WTG capacity) needs to be built while composed of an electrolyzer stack of 2500 individual electrolytic cells. This last design parameter (the number of alkaline electrolytic cells) prevents the plant to capture the total wind turbine capacity of 3 MW. When a larger plant size is generated by the genetic algorithm and the same number of electrolyzers is incorporated, the plant would be unable to operate at lower wind power due to the minimum current density (Figure 4). This set of design parameters would result in a lower annual ammonia production and therefore withdrawn from the set of optimal design parameters. The plant comprises of a load factor of 22.4%, which results by definition in a low

Table 2: Set of design parameters and results of the two extremities ('Most NH_3' and 'Best L_F') from the Pareto front. An increase in the NH_3 plant size (%NH_3size) increases the amount of electrolyzers (N) and the power distribution to the AWE section ($\%_{\text{AWE}}$). This small increase in the power distribution of the AWE relates to the non-linear behavior of the electrolyzer model at a larger power scale.

Design parameter		Case	
		Most NH_3	Best L_F
$\%_{\text{plantsize}}$	[%]	92.4	6.58
N	[-]	2500	954
$\%_{\text{AWE}}$	[%]	91.8	91.6
$\%_{\text{PSA}}$	[%]	1.60	1.60
Result			
$m_{\text{NH3,total}}$	[tonne]	491	122
L_F	[%]	22.4	73.5

utilization rate of the total plant, but for this design case, there is a potential to produce large amounts of ammonia that variate instantaneously with the wind speed. This would be an ideal way to capture the excessive power from the WTG. However, a commercial ammonia synthesis design is not adapted to this flexible functioning [9]. The observed pressure variations are problematic knowing that the ramp-up of the process is time limited (multiple hours to ramp-up the ammonia production) [41]. This could although be solved by accumulating hydrogen and nitrogen gas in storage tanks before the synthesis loop while supplying a constant mass flow of the mixture to the Haber-Bosch process. This makes the system less vulnerable to pressure changes if small fluctuations of power is guaranteed to this part of the plant.

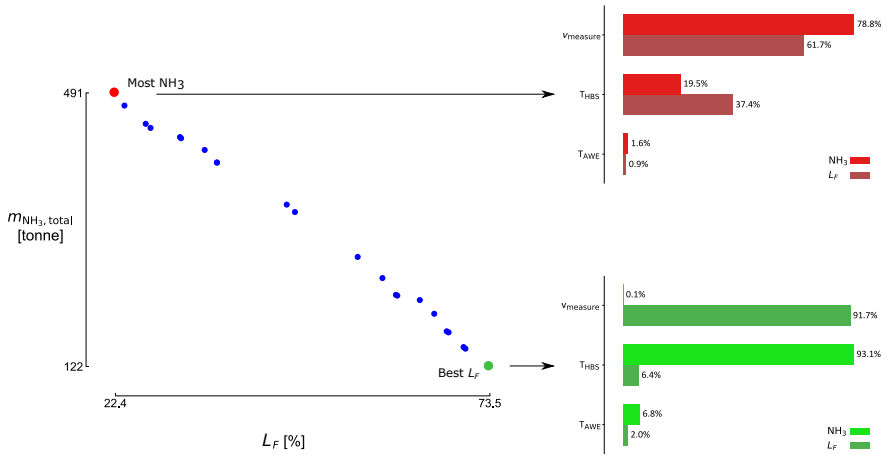

Figure 6: Maximizing the annual NH_3 production and the load factor (L_F) are conflicting objectives. One design can produce 491 tonne of NH_3 but has an L_F of 22.4% while another design produces 122 tonne of NH_3 with an L_F of 73.5%. The UQ analysis of the three operational uncertainties show, through the Sobol' indices, the dominance of the wind speed measurement (v_{measure}) influencing the load factor and the ammonia production in the 'Most NH_3' design. The reactor temperature (T_{HBS}) dominates the best L_F design in the ammonia production

For the design with the highest load factor ($L_F = 73.5\%$), the plant consumes 6.58% of the 3 MW WTG capacity (0.197 MW) while consisting of 954 electrolytic cells. A sensitivity analysis of this design showed that the NSGA-II algorithm established a plant design with a stable ammonia production and an electrolyzer stack performing at peak energy efficiency of 92.6% (Figure 4). This 'Best L_F' design produces a steady low flow of ammonia which is almost invulnerable to the variations of wind speed. This design type is the most common way to produce ammonia in combination with a grid connection to compensate for the absence of wind power [37], like the pilot plant in Minnesota [17]. Aside the stable production, the amount

of potential wind power discarded from the simulation (73.4% of the residual wind power) is unwanted when the principal use is equalizing the supply and demand of the electric grid. Complementary to the Haber-Bosch plant, the consumption of this residual excess energy in this case provides the necessity to install other flexible storage systems.

A global sensitivity analysis showed the effect of uncertainties applied on the two extreme cases together with the corresponding Sobol' indices (Figure 6). The UQ analysis provided a mean value for both objectives which was lower than their deterministic counterparts due to the adverse effect of the uncertainties on the total performance. The analysis applied on the 'Most NH_3' design resulted in a relative decrease of 0.62% in the ammonia production ($\mu_{\mathrm{NH_3,total}} = 488$ tonne NH_3) and a relative decrease in load factor by 6.63% ($\mu_{L_F} = 20.9\%$). The CoV of the NH_3 production and the load factor of the plant for the 'Most NH_3' case are respectively 1.57% and 7.46%. This result subsequently indicates that the load factor of this design is more affected by the variations of the uncertain parameters than the ammonia production. The UQ analysis of the 'Best L_F' design case presented a relative decrease of 0.56% in NH_3 production and 0.03% for L_F between the mean and the deterministic result, where the CoV of both outcomes in this case are respectively 0.70% and 0.07%. These values show that the deterministic design parameters for the best load factor design from the DDO analysis provides an ammonia plant that is insensitive to variations to the chosen uncertain parameters.

Regarding the Sobol' indices, the global sensitivity analysis shows the noise propagation due to the temperature variations in the NH_3 reactor and

the electrolytic cell, and the wind speed measurement error in the two cases for each objective (Figure 6). The temperature variations of the electrolyzer have in general less effect on the overall variance of the results (maximum 6.8% of the total variance in the 'Best L_F' design).

Different operational uncertainties influences the ammonia production in the two extreme cases. In the 'Most NH_3' case, the wind speed measurement error has a larger effect on the noise propagation of the NH_3 production (78.8%) than in the 'Best L_F' case (0.1%). The influence arises from the fact that the wind speed affects the generated power of the WTG, hence the consumed power by the ammonia plant; making the total NH_3 production more dependable on the wind speed. However in the 'Best L_F' case, the reactor temperature variations dominates the ammonia production (93.1%), while this uncertainty influences in the other case the result with only 19.5% of the total variance. This variation impacts the NH_3 production because of its effect on the equilibrium conditions in the ammonia reactor; directly controlling the amount of ammonia that is produced. The absence of the wind speed measurement error results from the objective to attain a high load factor, which ensures the continuous power flow to the plant; consequently minimizing the effect of the wind speed variation on the NH_3 production.

In the case of the load factor, the global sensitivity analysis shows that the wind speed variation has the largest contributions in both cases. This equivalent influence emerges with the definition of the load factor as our second optimization objective (Equation 8).

4.2. Robust design optimization

In the interest to find a design that enables the storage of wind power by the production of ammonia while minimizing the impact of the uncertainties on this production, a Robust Design Optimization (RDO) was performed on the model. Combining the NSGA-II algorithm and the PCE method provides a strategy to inexpensively measure the sensitivity of the outcome −or CoV− and progress towards a better set of design parameters, acquired by the genetic algorithm [40, 42, 43]. This approach optimized the wind-powered ammonia synthesis model to determine a design which maximizes the ammonia production while minimizing the CoV of this production.

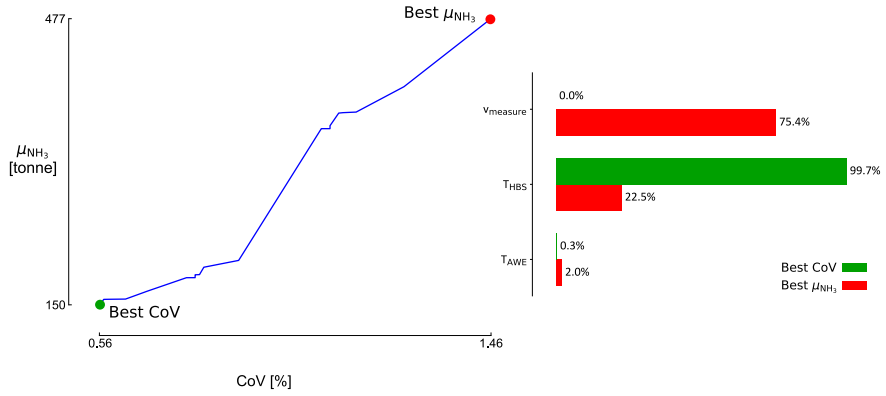

Figure 7: Maximizing the average NH_3 production and minimizing the Coefficient of Variance (CoV) are conflicting objectives. One design can produce 477 tonne of NH_3 but has a CoV of 1.46% while another design produces 150 tonne of NH_3 with a CoV of 0.56%. The NH_3 production of both RDO designs are influenced by the temperature variation of the ammonia reactor. In the 'Best CoV' case this variation dominates this result while the 'Best μ_{NH_3}' design is dominated by the wind speed variations.

Similar to DDO results, the RDO algorithm provided a trade-off between

the two chosen objectives, where two extremities each secure a unique set of design parameters to reach a specific objective (Figure 7). In the most robust case ('Best CoV'), the energy storage system produces on average low quantities of ammonia (150 tonne of NH_3 annually) but consists of a CoV which is 2.6 times lower than the conflicting optimal design. This conflicting case ('Best μ_{NH_3}') delivers a 3.18 times higher mean production (477 tonne of NH_3 on average) than the 'Best CoV' design. These two opposing designs have a key design parameter which determines this difference in production, namely the fraction of power allowed from the 3 MW wind turbine (i.e. the power plant size). This crucial design parameter creates this trade-off of robustification (Table 3). In comparison with the obtained DDO design parameters (Table 2), the RDO design parameters have a similar design configuration with the 'Most NH_3' case of the DDO process. This shows that the exploration and exploitation of the Latin Hypercube and NSGA-II algorithm reaches the same results for the same objective in the different optimization cases. The Gaussian uncertainties causes the different ammonia productions.

A global sensitivity analysis of the NH_3 production applied on the two extreme trade-off designs resulted in the individual variance of each operational uncertainty presented through the Sobol' indices (Figure 7). According to these Sobol' indices, a different operational uncertainty influences the ammonia production of the two designs. In the 'Best CoV' (most robust) design case, the temperature variations of the ammonia reactor dominates this results. If the objective is to create a robust ammonia plant, the temperature variations of the reactor needs to be smaller. Jinasena et al. already pro-

Table 3: Set of design parameters and results of the two extremities ('Best μ_{NH_3}' and 'Best CoV') from the Pareto front established by the RDO process. The NH_3 plant size ($\%_{plantsize}$) is the key design parameter for composing a robust ammonia plant.

Design parameter		Case	
		Best μ_{NH_3}	Best CoV
$\%_{plantsize}$	[%]	85.7	11.4
N	[-]	2490	2339
$\%_{AWE}$	[%]	91.9	92.5
$\%_{PSA}$	[%]	1.59	1.23
Result			
μ_{NH_3}	[tonne]	477	150
CoV	[%]	1.46	0.56

vided examples on how to stabilize temperature fluctuations by increasing the monitoring measurements of the heat exchanger that controls the incoming flow. These measurements consisted of analyzing the composition of feed gases, feed flow rate, reactor inlet temperature and the pressure along the reactor [34].

In the other case ('Best μ_{NH_3}'), a plant design is obtained with a CoV of 1.46% and an annual ammonia production of 477 tonne which is mostly influenced by the wind speed measurement error and (in smaller quantities) the temperature of the HBS reactor. The impact of the accuracy of the wind speed can be reduced by implementing a more accurate wind speed measurement device and a better calibration/positioning of the anemometer.

As in the deterministic optimization, the temperature variations of the AWE have little effect on the performance of the ammonia plant although

91.9% of the consumed power goes to the alkaline electrolyzer for the production of H_2.

5. Conclusion

This paper provided the steady-state modeling and optimization of an NH_3-based energy storage system in Aspen Plus® based on the expected wind power production from a designed WTG in Python. The integrated WTG powered the AWE, PSA and HBS compressor in a certain ratio, so the storage of wind energy through ammonia production could be optimized by the applied multi-objective optimization approach, i.e. the NSGA-II algorithm. Adjacent to the modeling of these subsystems, we identified and integrated the wind speed measurement error, the temperature variation of the electrolyzer and the NH_3 synthesis reactor as the operational uncertainties. The PCE algorithm measured the uncertainty propagation of these operational uncertainties when analyzing a certain objective. The multi-objective DDO consisted of maximizing the ammonia production and the plants load factor with the NSGA-II algorithm. In the RDO step, the optimization and robustification of this ammonia production was requested from the NSGA-II algorithm in combination with the PCE method.

The DDO step provided a Pareto front where its outer ends delivered a productive and high load factor design. The key difference between these two designs to allow the capture of the wind energy and the continuous operation of the system, arises from two design variables; the sizing of the total storage system and the number of electrolytic cells. A global sensitivity analysis on each objective showed that the temperature variations of the ammonia

reactor and the wind speed measurement influences the load factor, while the NH_3 production is either dominated by the wind speed measurement or by the temperature fluctuation in the ammonia reactor. The integrated temperature variations in the AWE has little influence on the noise on each DDO objective.

Similar to the DDO case, the robust optimization procedure delivered a trade-off between a productive and a robust design. The key design parameter for obtaining either one of the two designs lies within the sizing of the total storage system. A larger sized storage system grants the opportunity to produce higher amounts of ammonia but is subjected to the uncertainty of the wind speed measurement and the temperature fluctuation in the ammonia reactor. In contrast to this productive design, the most robust design provides annually lower quantities of ammonia, but is only subjected to the temperature fluctuation of the ammonia reactor and in smaller proportion to the temperature variation in the AWE. Implementing a more accurate wind speed measurement device and increasing the monitoring measurements of the heat exchanger that controls the incoming flow towards the HBS reactor can decrease the CoV on the NH_3 production in both RDO cases. A future investigation will involve analyzing the dynamical operations of the power-to-ammonia pathway and robustifying its levelized cost.

Acknowledgments

The work has been performed in the scope of the GenComm project, funded by Interreg North-West Europe. Aspen Plus was used under academic licenses.

Appendix A. Parameters alkaline water electrolyzer

Table A.4: Model parameters of the AWE located in the PHOEBUS plant operating at a pressure of 7 bar and a temperature between 30 and 80°C [30].

U-I design parameters		Value
r_1	[Ωm^2]	7.33110^{-5}
r_2	[Ωm^2 $^oC^{-1}$]	-1.1010^{-7}
s_1	[V]	1.58610^{-1}
s_2	[V $^oC^{-1}$]	1.37810^{-3}
s_3	[V $^oC^{-2}$]	-1.60610^{-5}
t_1	[m^2A^{-1}]	1.59910^{-2}
t_2	[m^2A^{-1} $^oC^{-1}$]	-1.302
t_3	[m^2A^{-1} $^oC^{-2}$]	421.310^2
A	[m^2]	0.25
η_F design parameters		
f_1	[%]	99.5
f_2	[m^2A^{-1}]	-9.5788
f_3	[m^2A^{-1} $^oC^{-1}$]	-0.0555
f_4	[m^4A^{-1}]	1502.7083
f_5	[m^4A^{-1} $^oC^{-1}$]	-70.8005

References

[1] M. Lott, S.-I. Kim, C. Tam, D. Elzinga, S. Heinen, L. Munuera, U. Remme, Technology Roadmap: Energy storage, International Energy Agency (2014) 64.

[2] A. Evans, V. Strezov, T. J. Evans, Assessment of utility energy storage options for increased renewable energy penetration, Renewable and Sustainable Energy Reviews 16 (2012) 4141–4147.

[3] G. Wang, A. Mitsos, W. Marquardt, Conceptual design of ammonia-based energy storage system: System design and time-invariant performance, AIChE Journal 63 (2017) 1620–1637.

[4] F. Díaz-González, A. Sumper, O. Gomis-Bellmunt, R. Villafáfila-Robles, A review of energy storage technologies for wind power applications, Renewable and Sustainable Energy Reviews 16 (2012) 2154–2171.

[5] C. Wulf, J. Linßen, P. Zapp, Review of Power-to-Gas Projects in Europe, Energy Procedia 155 (2018) 367–378.

[6] M. Kopp, D. Coleman, C. Stiller, K. Scheffer, J. Aichinger, B. Scheppat, Energiepark Mainz: Technical and economic analysis of the worldwide largest Power-to-Gas plant with PEM electrolysis, International Journal of Hydrogen Energy 42 (2017) 13311–13320.

[7] G. Guandalini, M. Robinius, T. Grube, S. Campanari, D. Stolten, Long-term power-to-gas potential from wind and solar power: A country analysis for Italy, International Journal of Hydrogen Energy 42 (2017) 13389–13406.

[8] WaterstofNet to lead European hydrogen truck project H2-Share, Fuel Cells Bulletin 2017 (2017) 3.

[9] Institute for Sustainable Process Technology, Power to Ammonia, Technical Report, ISPT, 2017.

[10] U. Bossel, B. Eliasson, Energy and the Hydrogen Economy, ABB Switzerland Ltd (2009) 1–35.

[11] J. Fuhrmann, M. Hülsebrock, U. Krewer, Energy Storage Based on Electrochemical Conversion of Ammonia, in: Transition to Renewable Energy Systems, Wiley-VCH Verlag GmbH & Co. KGaA, Weinheim, Germany, 2013, pp. 691–706.

[12] I. I. Cheema, U. Krewer, Operating envelope of Haber–Bosch process design for power-to-ammonia, RSC Advances 8 (2018) 34926–34936.

[13] E. Morgan, J. Manwell, J. McGowan, Wind-powered ammonia fuel production for remote islands: A case study, Renewable Energy 72 (2014) 51–61.

[14] R. Bañares-Alcántara, G. Dericks III, M. Fiaschetti, P. Grünewald, J. Masa Lopez, E. Tsang, A. Yang, L. Ye, S. Zhao, Analysis of Islanded Ammonia-based Energy Storage Systems, Technical Report, University of Oxford, Oxford, 2015.

[15] D. Frattini, G. Cinti, G. Bidini, U. Desideri, R. Cioffi, E. Jannelli, A system approach in energy evaluation of different renewable energies sources integration in ammonia production plants, Renewable Energy 99 (2016) 472–482.

[16] A. Valera-Medina, H. Xiao, M. Owen-Jones, W. I. David, P. J. Bowen, Ammonia for power, Progress in Energy and Combustion Science 69 (2018) 63–102.

[17] M. Reese, C. Marquart, M. Malmali, K. Wagner, E. Buchanan, A. McCormick, E. L. Cussler, Performance of a Small-Scale Haber Process, Industrial & Engineering Chemistry Research 55 (2016) 3742–3750.

[18] I. Wilkinson, Siemens green Ammonia, 1st NH3 European event, Netherlands: Rotterdam, 2017.

[19] M. Aziz, T. Oda, A. Morihara, T. Kashiwagi, Combined nitrogen production, ammonia synthesis, and power generation for efficient hydrogen storage, Energy Procedia 143 (2017) 674–679.

[20] K. E. Lamb, M. D. Dolan, D. F. Kennedy, Ammonia for hydrogen storage; A review of catalytic ammonia decomposition and hydrogen separation and purification, International Journal of Hydrogen Energy 44 (2019) 3580–3593.

[21] K. Deb, A. Pratap, S. Agarwal, T. Meyarivan, A fast and elitist multiobjective genetic algorithm: NSGA-II, IEEE Transactions on Evolutionary Computation 6 (2002) 182–197.

[22] S. Abraham, M. Raisee, G. Ghorbaniasl, F. Contino, C. Lacor, A robust and efficient stepwise regression method for building sparse polynomial chaos expansions, Journal of Computational Physics 332 (2017) 461–474.

[23] sotaventogalicia.com, Real time data, ???? [Online]. Available: `http://www.sotaventogalicia.com/en/real-time-data/historical`. [Accessed: 2 May 2018].

[24] Wind-turbine-models.com, Vestas V112 onshore wind turbine, ???? URL: https://bit.ly/2M9xCwL.

[25] E. I. Kaganov, A. M. Yaglom, Errors in wind-speed measurements by rotation anemometers, Boundary-Layer Meteorology 10 (1976) 15–34.

[26] N. Boccard, Capacity factor of wind power realized values vs. estimates, Energy Policy 37 (2009) 2679–2688.

[27] M. A. Lackner, A. L. Rogers, J. F. Manwell, Uncertainty Analysis in MCP-Based Wind Resource Assessment and Energy Production Estimation, Journal of Solar Energy Engineering 130 (2008) 031006.

[28] A. Buttler, H. Spliethoff, Current status of water electrolysis for energy storage, grid balancing and sector coupling via power-to-gas and power-to-liquids: A review, Renewable and Sustainable Energy Reviews (2017).

[29] J. Proost, State-of-the art CAPEX data for water electrolysers, and their impact on renewable hydrogen price settings, International Journal of Hydrogen Energy (2018).

[30] Ø. Ulleberg, Stand-alone power systems for the future: optimal design, operation & control of solar-hydrogen energy systems, NTNU, Trondheim, Norvège (1998).

[31] M. Mori, T. Mržljak, B. Drobnič, M. Sekavčnik, Integral characteristics of hydrogen production in alkaline electrolysers, Strojniski Vestnik/Journal of Mechanical Engineering 59 (2013) 585–594.

[32] B. Fastrup, H. Nygård Nielsen, On the influence of oxygen on iron catalysts during ammonia synthesis and catalyst characterization, Catalysis Letters 14 (1992) 233–239.

[33] E. R. Morgan, Techno-Economic Feasibility Study of Ammonia Plants Powered by Offshore Wind, Ph.D. thesis, 2013.

[34] A. Jinasena, B. Lie, B. Glemmestad, Dynamic Model of an Ammonia Synthesis Reactor based on Open Information, in: Proceedings of The 9th EUROSIM Congress on Modelling and Simulation, EUROSIM 2016, The 57th SIMS Conference on Simulation and Modelling SIMS 2016, volume 142, 2018, pp. 998–1004.

[35] M. S. Mudahar, T. P. Hignett, Energy efficiency in nitrogen fertilizer production, Energy in Agriculture 4 (1985) 159–177.

[36] L. Tock, F. Maréchal, M. Perrenoud, Thermo-environomic evaluation of the ammonia production, The Canadian Journal of Chemical Engineering 93 (2015) 356–362.

[37] C. Philibert, Producing ammonia and fertilizers: new opportunities from renewables, ee.co.za (????).

[38] M. Stein, Large sample properties of simulations using latin hypercube sampling, Technometrics 29 (1987) 143–151.

[39] B. Sudret, Polynomial chaos expansions and stochastic finite-element methods, 2003, 2014.

[40] D. Coppitters, W. De Paepe, F. Contino, Surrogate-assisted robust design optimization and global sensitivity analysis of a directly coupled photovoltaic-electrolyzer system under techno-economic uncertainty, Applied Energy 248 (2019) 310–320.

[41] A. Allman, P. Daoutidis, Optimal scheduling for wind-powered ammonia generation: Effects of key design parameters, Chemical Engineering Research and Design 131 (2018) 5–15.

[42] P. Tsirikoglou, S. Abraham, F. Contino, Ö. Bağci, J. Vierendeels, G. Ghorbaniasl, Comparison of metaheuristics algorithms on robust design optimization of a plain-fin-tube heat exchanger, in: 18th AIAA/ISSMO Multidisciplinary Analysis and Optimization Conference, American Institute of Aeronautics and Astronautics, Reston, Virginia, 2017.

[43] W. D. Paepe, D. Coppitters, S. Abraham, P. Tsirikoglou, G. Ghorbaniasl, F. Contino, Robust Operational Optimization of a Typical micro Gas Turbine, Energy Procedia 158 (2019) 5795–5803.